Physics in Medicine &
Biology

PAPER • OPEN ACCESS

Gadolinium oxide nanoparticles as a multimodal contrast enhancement agent for pre-clinical proton imaging

To cite this article: Matthias Würl *et al* 2025 *Phys. Med. Biol.* **70** 025013

IOP Publishing Phys. Med. Biol. 70 (2025) 025013 https://doi.org/10.1088/1361-6560/ada5a4

Physics in Medicine & Biology

IPEM Institute of Physics and Engineering in Medicine

OPEN ACCESS

RECEIVED
30 December 2023

REVISED
18 December 2024

ACCEPTED FOR PUBLICATION
3 January 2025

PUBLISHED
17 January 2025

PAPER

Gadolinium oxide nanoparticles as a multimodal contrast enhancement agent for pre-clinical proton imaging

Matthias Würl[1], Grigory Liubchenko[1], Guyue Hu[1], Katrin Schnürle[1], Sebastian Meyer[1,6], Jonathan Bortfeldt[1], Guillaume Landry[1,2], Lukas Käsmann[2], Kirsten Lauber[2], Carlos Granja[3], Cristina Oancea[3], Enrico Verroi[4], Francesco Tommassino[4,5] and Katia Parodi[1,*]

[1] Department of Medical Physics, Ludwig-Maximilians-Universität München, Garching b. München, Germany
[2] Department of Radiation Oncology, University Hospital, LMU Munich, Munich, Germany
[3] ADVACAM s.r.o, Prague, Czech Republic
[4] INFN TIFPA, Trento, Italy
[5] University of Trento, Trento, Italy
[6] Present address: Department of Medical Physics, Memorial Sloan Kettering Cancer Center, New York, United States of America.
[*] Author to whom any correspondence should be addressed.

E-mail: katia.parodi@physik.uni-muenchen.de

Keywords: proton imaging, proton therapy, nanoparticles, contrast agent, small animal irradiation

Abstract

Orthotopic tumor models in pre-clinical translational research are becoming increasingly popular, raising the demands on accurate tumor localization prior to irradiation. This task remains challenging both in x-ray and proton computed tomography (xCT and pCT, respectively), due to the limited contrast of tumor tissue compared to the surrounding tissue. We investigate the feasibility of gadolinium oxide nanoparticles as a multimodal contrast enhancement agent for both imaging modalities. We performed proton radiographies at the experimental room of the Trento Proton Therapy Center using a MiniPIX-Timepix detector and dispersions of gadolinium oxide nanoparticles in sunflower oil with mass fractions up to 8wt%. To determine the minimum nanoparticle concentration required for the detectability of small structures, pCT images of a cylindrical water phantom with cavities of varying gadolinium oxide concentration were simulated using a dedicated FLUKA Monte Carlo framework. These findings are complemented by simulating pCT at dose levels from 80 mGy to 320 mGy of artificially modified murine xCT data, mimicking different levels of gadolinium oxide accumulation inside a fictitious tumor volume. To compare the results obtained for proton imaging to x-ray imaging, cone-beam CT images of a cylindrical PMMA phantom with cavities of dispersions of oil and gadolinium oxide nanoparticles with mass fractions up to 8wt% were acquired at a commercial pre-clinical irradiation setup. For proton radiography, considerable contrast enhancement was found for a mass fraction of 4wt%. Slightly lower values were found for the simulated pCT images at imaging doses below 200 mGy. In contrast, full detectability of small gadolinium oxide loaded structures in xCT at comparable imaging dose is already achieved for 0.5wt%. Achieving such concentrations required for pCT imaging inside a tumor volume in *in-vivo* experiments may be challenging, yet it might be feasible using different targeting and/or injection strategies.

1. Introduction

Small animal models are widely used in pre-clinical translational research to investigate the response of tumors and normal tissue to radiation therapy and other treatment modalities. Thereby, orthotopic tumor models are becoming increasingly popular compared to frequently used subcutaneous models, as they enable the study of the interplay with surrounding tissue in the correct environment. However, due to the deeper implantation, reliable tumor localization is generally more challenging and demands high precision for pre-clinical irradiation of orthotopic tumor models (Verhaegen *et al* 2011).

Several commercial and non-commercial image-guided small animal x-ray or proton irradiation platforms have been developed within the past few years, or are being currently developed (Verhaegen *et al* 2011, Tillner *et al* 2016, Kim *et al* 2019, Parodi *et al* 2019). Pre-treatment imaging is generally performed with an on-board or closeby cone-beam computed tomography (CBCT) unit or microCT imager. For proton irradiation platforms, an appealing alternative to x-ray CT (xCT) is to utilize an on-board proton CT (pCT) scanner such that the same radiation quality is used both for imaging and treatment. This allows for the direct determination of the relative (to water) stopping power (RSP), which is required for accurate dose calculation.

For orthotopic tumor models, the localization for target volume definition and for precise volume follow-up after treatment is challenging in xCT scans, raising the interest in using contrast enhancement agents (Stegen *et al* 2020). Although pCT may provide better density resolution as compared to xCT (Cormack and Koehler 1976, Schulte *et al* 2005, Meyer 2019), tumor localization in pCT images can also benefit from the administration of suitable contrast enhancement agents.

In the past two decades, metallic nanoparticles have attracted attention in the field of radiation therapy for diagnostic, therapeutic and theranostic applications (Schuemann *et al* 2020). Most prominent to date are gold nanoparticles, which due to their non-toxicity have been studied as radiosensitizers for x-ray and proton radiation therapy (Hainfeld *et al* 2004, Lin *et al* 2014). Their high x-ray attenuation coefficient offers great potential as contrast enhancement agent for x-ray based imaging (Hainfeld *et al* 2006, Cole *et al* 2015) and the large (electron) density can improve contrast and hence tumor visualization in proton imaging (Schulte *et al* 2004, Meyer 2019, Sidebottom *et al* 2021). Another frequently investigated element to be used as metallic nanoparticles for imaging and radiation therapy is the lanthanide Gadolinium. In molecular form, it has been used in clinics as contrast agent for magnetic resonance imaging (MRI) since the 1980s. With an atomic number of 64, it is comparable to gold ($Z = 79$) when it comes to enhancement of radiosensitivity and imaging contrast in x-ray imaging. In fact, the multimodal imaging capability of gadolinium (oxide) based nanoparticles for fluorescent imaging, xCT and MRI has already been shown in various studies, both *in-vitro* and *in-vivo* (Bridot *et al* 2007, Ahmad *et al* 2015, Rajaee *et al* 2019), and the first gadolinium-based nanoparticles (AGuIX®) have recently been approved for clinical trials (Verry *et al* 2019).

In this work, we further explore the feasibility of gadolinium oxide nanoparticles as a multimodal contrast enhancement agents in CBCT as well as proton radiography (pRad) and pCT in the context of small animal imaging. It is important to emphasize that possible biological effects of the administration of gadolinium oxide nanoparticles are beyond the scope of this study. Instead, this study focusses on the potential benefits and possible threshold values from an imaging point of view. We therefore restrict ourselves to pRad experimental studies in phantoms, along with in-silico pCT imaging based on murine CBCT image, in which gadolinium oxide nanoparticles are loaded by artificially modifying the tissue composition in fictitious tumor volumes prior to simulation of the imaging workflow.

2. Materials and methods

2.1. Contrast-enhanced proton radiography

The feasibility of contrast enhancement using gadolinium oxide nanoparticles for proton radiography was investigated at the physics beamline in the experimental room of the Trento Proton Therapy Center (Trento PTC) of azienda provinciale servizi sanitari (APSS) (Tommasino *et al* 2017). Proton radiographies were acquired with a mono-energetic proton beam of 70.2 MeV and a miniaturized radiation camera MiniPIX-Timepix *(ADVACAM s.r.o, Prague, Czech Republic)* (Granja *et al* 2018, Olsansky *et al* 2022).

2.1.1. Phantom

Gadolinium oxide nanoparticles with an average particle size of 15–30 nm were purchased from a commercial vendor *(Ionic Liquids Technologies GmbH, Heilbronn, Germany)*. Since these nanoparticles tend to agglomerate and settle within a few minutes when dispersed in water, dispersions of nanoparticles in sunflower oil were prepared. The considerably higher viscosity retarded settling, providing a more homogeneous mixture throughout the imaging time of up to 15 min. Three dispersions with gadolinium oxide mass fractions of 4wt%, 6wt% and 8wt% were produced. A PMMA cuboid ($8 \times 2 \times 3\,\mathrm{cm}^3$) with 4 cylindrical vessels (1 cm diameter, 2 cm height) served as container for the dispersions. Although the phantom design would allow to simultaneously fill the cavities with up to 4 different mixtures, only one vessel was sequentially used for all mixtures due to the limited field-of-view of the detector.

2.1.2. Detection setup and acquisition

The proton radiography setup used in this study is described in detail in Würl *et al* (2020). It relies on the measurement of position and energy loss in the sensitive detector volume for individual protons after

traversing the phantom. The used MiniPIX-Timepix detector features a 300 μm thick silicon sensor chip and is based on the hybrid semiconductor pixel detector Timepix ASIC chip (Llopart *et al* 2007) with a sensitive area of $14.08 \times 14.08\,\mathrm{mm}^2$ (256×256 energy sensitive pixels of 55 μm pitch). It was biased at +30 V and a frame acquisition time of 40 ms was used. Measurements were performed in Time-over-Threshold (ToT) mode and pixel values were converted to energy deposition in keV using a previously performed per-pixel calibration (Jakubek 2011).

The imaging setup and is show in figures 1(a) and (b). The MiniPIX detector was aligned with its sensor surface in the isocenter of the experimental room using the in-room laser alignment system. The PMMA phantom was placed 1 cm upstream of the detector to reduce degradation of the spatial resolution due to scattering. The filled cavity was centered with respect to the beam spot and the sensor area. Radiographies were acquired subsequently for the cavity filled with pure sunflower oil and the three dispersions.

From the position and energy loss measurement of individual protons, two-dimensional water-equivalent thickness (WET) images were determined as described in Würl *et al* (2020). In short, all registered events were spatially binned ($0.2 \times 0.2\,\mathrm{mm}^2$ image pixel size) and filtered according to user-specified criteria to sort out bad events. For each image pixel, the per-pixel median energy deposition of all good events was converted to WET using a dedicated conversion curve, which was based on FLUKA (Ferrari *et al* 2005, Böhlen *et al* 2014) Monte Carlo (MC) simulations and tuned using experimental measurements. The resulting WET images were median-filtered (kernel size 5×5 pixel) to reduce per-pixel fluctuations.

A supplementary MC simulation was used to estimate the imaging dose per radiography and was found to be around 2 mGy, reaching up to 4 mGy in the center of the field-of-view due to the relatively small beam spot size ($\sigma = 7.1$ mm) and the consequential fluence inhomogeneity.

2.2. pCT MC simulation study

An initial assessment of the feasibility of using gadolinium oxide nanoparticles to enhance the visibility of small features in proton imaging in an extensive FLUKA MC simulation study (version 2020.0.3, HADROTHE defaults) (Ferrari *et al* 2005, Böhlen *et al* 2014) is presented in this work. We used the in-silico implementation of a single particle tracking, small animal pCT system (Meyer *et al* 2020) and a 75 MeV proton pencil beam from a clinical beamline (Würl *et al* 2016). The pCT system consists of two Micromegas based tracking detectors respectively upstream and downstream of the imaged object and a residual range telescope based on a segmented time projection chambers (TPC) with 70 interleaved 500 μm thick Mylar absorbers. A schematic view of the setup is shown in figure 1(c).

The imaged objects, described in the subsequent paragraphs, were rotated with respect to the beam axis and the detectors such that for each object 180 independent simulations for equally spaced angles between 0 and 360 degrees were performed. Each simulation generated a list-mode data set of position and direction in the two tracking detectors and the residual range from the TPC range telescope, along with a voxelized dose scoring inside the object. For the tomographic reconstruction of the RSP, we used a C++ implementation of the ordered subset simultaneous algebraic reconstruction technique with total variation superiorization (TVS OS-SART) (Meyer 2019, Hu 2021). Straight line paths of the protons through the object were assumed since for murine-sized objects a comparison to cubic spline path had not shown any advantage of the more computationally demanding model (Meyer 2019). The final RSP images were reconstructed on a $0.2 \times 0.2 \times 0.2\,\mathrm{mm}^3$ voxel grid.

2.2.1. Cylindrical water phantom

For the first pCT contrast enhancement study, we used a cylindrical water phantom (30 mm diameter) with eight cylindrical cavities (4 mm diameter) containing a varying gadolinium oxide mass fraction, approximating a homogeneous distribution of nanoparticles in water. One cavity was filled with pure water, in the other vessels the gadolinium oxide mass fraction was ranging from 2wt% up to 8wt%. The densities of the mixtures were adjusted according to their mass and volume increase. A total of 3.7×10^6 primary protons were simulated for each projection. This results in an imaging dose of 200 mGy for the full tomography, being in the same order as current CBCT or micro-CT scans for pre-clinical research (Verhaegen *et al* 2018). To assess the impact of gadolinium oxide traces in the surrounding medium on the detectability of the small features, additional pCT simulations with a water-nanoparticle mixture of 0.2 wt% in lieu of pure water were performed (Cho *et al* 2009, Meyer 2019). The central three slices were reconstructed and selected for further quantitative evaluation. Additional tomographies including only half of the simulated proton tracks were reconstructed to mimic pCT with a reduced imaging dose of 100 mGy.

2.2.2. pCT simulation using murine xCT image

In order to study the feasibility of contrast enhancement by gadolinium oxide nanoparticles in a scenario that is more realistic and relevant for pre-clinical imaging, the cylindrical phantom was replaced by a

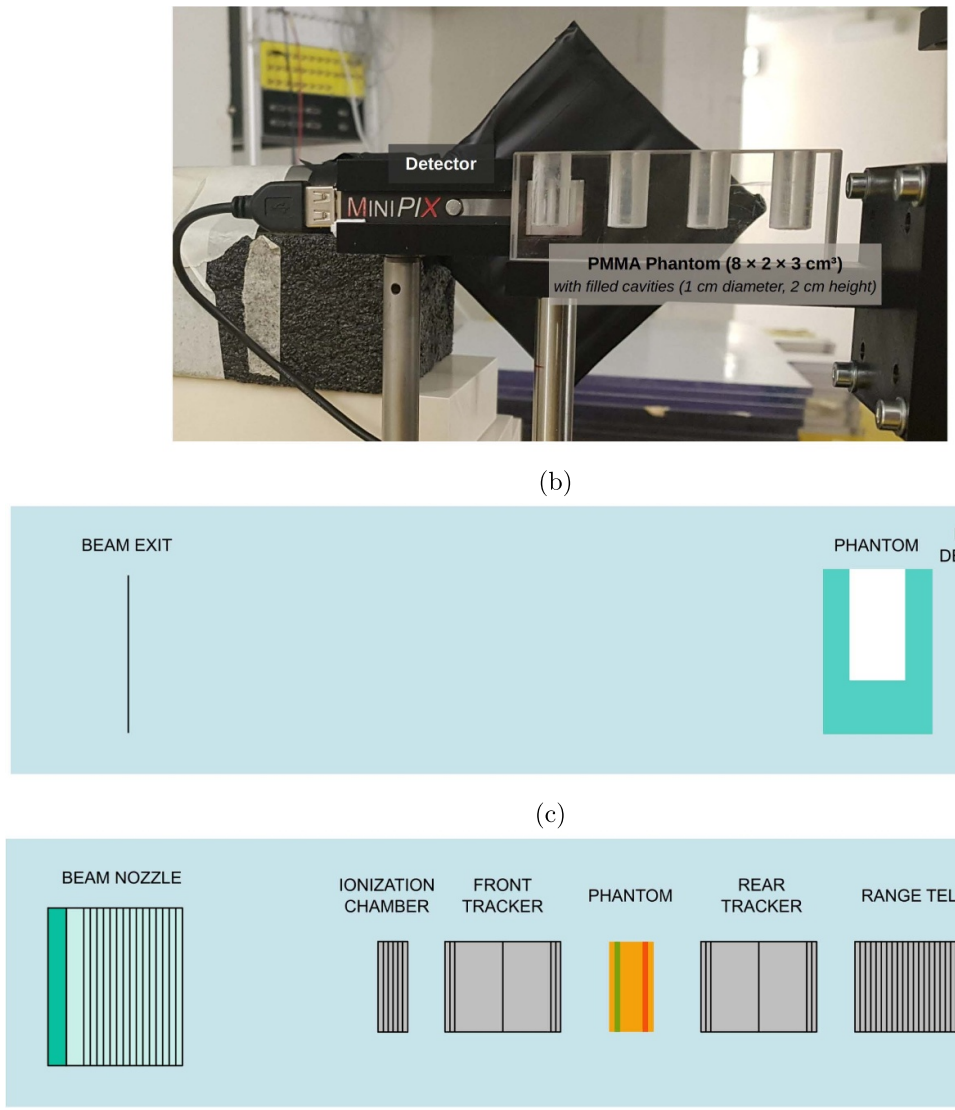

Figure 1. (a) Setup for proton radiography in beam's eye view. The PMMA phantom with cylindrical cavities is placed 1 cm upstream of the MiniPIX-Timepix detector with silicon sensor of 14.08 × 14.08 mm^2. A schematic view of the experimental pRad setup and the pCT Monte Carlo simulation setup is shown in (b) and (c), respectively.

voxelized murine CT image. To this end, a native CBCT image of an anesthesized mouse, acquired in the scope of another study using a small animal radiation research platform (SARRP, X-Strahl, Camberley, Great Britain) (Wong *et al* 2008), served as input for the simulation study. The FLUKA user interface Flair (Vlachoudis 2009) was used to create a voxelized geometry from the CBCT scan by converting CT numbers in Hounsfield units (HU) into materials with specific densities and elemental compositions (Parodi *et al* 2007, Kozł owska *et al* 2019). Since the xCT scan was acquired without injection of any contrast agent, the DICOM data was artificially modified to mimic accumulation of nanoparticles inside a fictitious, spherical tumor volume of 113 mm^3. CT numbers of the original DICOM image within this region were replaced by 4500, which is far beyond typical HU values found in such CT images. For the conversion of HU to material, an additional, new material was hence defined for that HU interval (>3250). Note that the chosen CT number of this nanoparticle loaded tumor volume is not related to the actually expected HU value, but merely serves to unambiguously attribute the correct material in the conversion of HU to material. The atomic composition and mass density of this material was based on the material definition of the HU interval (120, 200], which was the predominant interval in the region-of-interest of the original CBCT image. A mass fraction gadolinium oxide of 4wt%, 6wt% and 8wt% was added to the atomic composition and the mass density in subsequent simulations. For calculating the contrast-to-noise ratio (see section 2.4), the respective

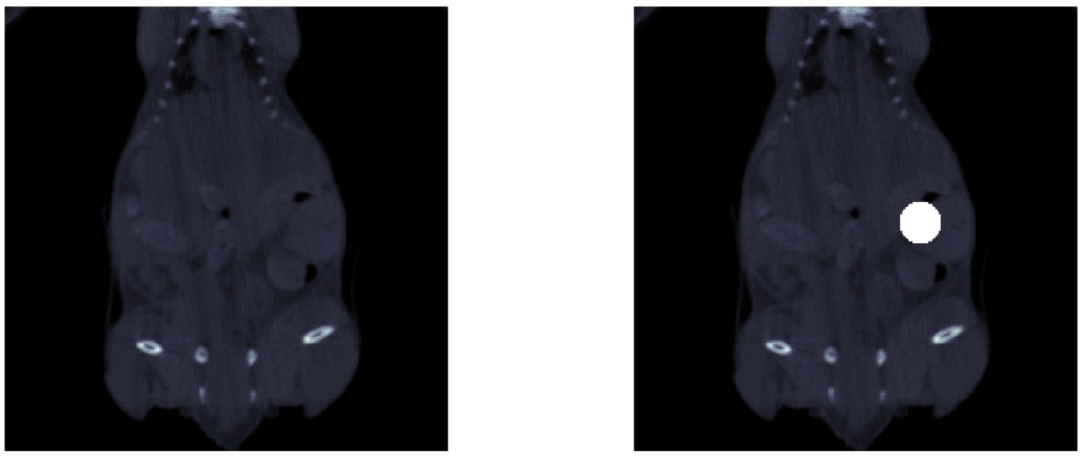

Figure 2. Coronal view through the original (a) and modified (b) murine xCT, including the fictitious tumor volume assigned with the elevated HU value of 4500.

voxel values were overwritten by the mean CT number of the surrounding tissue (160 HU) to additionally simulate pCT without contrast agent, using the standard segmentation approach. A coronal view through the original murine xCT and the modified xCT images is shown in figure 2.

pCT simulations were performed using 6×10^6 protons per projection, resulting in an imaging dose of 320 mGy for the full tomography of 180 projections. Images were reconstructed for the full dose, as well as for 160 mGy and 80 mGy by using only half and a quarter of the simulated proton tracks, respectively. For each imaging dose and gadolinium oxide mass fraction, five central slices were reconstructed and further evaluated.

2.3. Contrast enhancement in x-ray CBCT imaging

To investigate the potential of gadolinium oxide nanoparticles as a multimodal contrast enhancement agents in a pre-clinical scenario, x-ray CBCT images of a cylindrical PMMA phantom (20 mm diameter, 40 mm height) were acquired using the SARRP installed at the Department of Radiation Oncology of the University Hospital of the LMU Munich. PMMA was chosen as a widely used surrogate material for water, easy to manufacture and handle, as well as cost-effective. The phantom dimension was reduced compared to the initial theoretical proton imaging study in water to provide a size which could also be compatible to future proton tomographic imaging experiments using beam energies down to 70 MeV, once the investigated proton imaging prototype of Meyer *et al* (2020) will be completed and become operational. The phantom had 5 cylindrical cavities (3.3 mm diameter, 30 mm height) filled with dispersions of 0.5wt%, 2wt%, 4wt% and 8wt% gadolinium oxide in sunflower oil, as well as pure sunflower oil. The lower mass fraction as compared to proton imaging was chosen since increased contrast enhancement was expected.

The CBCT scan was acquired with 1440 projections with x-ray tube settings of 60 kVp and 0.8 mA and a 1 mm aluminum filter. Although the imaging dose was not directly measured, a comparison with other studies (Yang *et al* 2015, Johnstone and Bazalova-Carter 2018) using similar tube settings indicates that the dose likely ranged from several tens to 200 mGy, which is comparable to the phyical doses applied in our pCT simulations.

Raw projections were exported and images were reconstructed using an in-house implementation of the Feldkamp–David–Kress algorithm (Feldkamp *et al* 1984) with a voxel size of $0.26 \times 0.26 \times 0.26\,\mathrm{mm}^3$. It is worth considering that the HU values obtained with CBCT may be subject to some uncertainty due to factors such as beam hardening, phantom positioning within the scanner's field of view, and the presence of artifacts. However, in our study, the selected phantom design and consistent positioning within the scanner resulted in a HU uncertainty which is small compared to its variance.

2.4. Metric for image analysis

Similar to Dunning and Bazalova-Carter (2020), the detectability and the minimum required gadolinium oxide mass fraction was estimated by calculating the contrast-to-noise ratio (CNR) according to

$$\mathrm{CNR} = \frac{|\mu_{\mathrm{ROI}} - \mu_{\mathrm{BG}}|}{\sigma_{\mathrm{BG}}}, \tag{1}$$

where μ_{ROI} is the mean signal value (RSP for pCT, HU for xCT) of the nanoparticle loaded regions-of-interest (ROIs). μ_{BG} and σ_{BG} are respectively the mean signal and standard deviation of the cavity filled with pure water/oil. For the pCT simulation with gadolinium oxide traces in the surrounding medium, the cavity with the 0.2wt% mixture was chosen as background region. To decouple detectability from spatial resolution, a margin of 1 mm and 0.5 mm was used for the definition of the ROIs for pCT and xCT images, respectively. The CNR uncertainty was calculated by replacing the numerator in equation (1) by $\sqrt{\sigma_{ROI}^2 + \sigma_{BG}^2}$. For detectability of the feature of interest, a CNR $\geqslant 5$ was considered according to the Rose criterion (Rose 1973, Burgess 1999). The corresponding minimum gadolinium oxide mass fraction was determined by applying a linear fit to the CNR vs. mass fraction.

3. Results

3.1. Contrast-enhanced proton radiography

Proton radiographies obtained at the Trento PTC using the MiniPIX-based imaging setup are shown in in figure 3(a) for pure sunflower oil and gadolinium oxide nanoparticle dispersions with mass fractions of 4wt%, 6wt% and 8wt%, respectively. WET values of the central 1 mm wide region (i.e. 5 pixels) along the cylindrical cavity axis were averaged and the resulting line profiles are shown in figure 3(b). Since for the different nanoparticle concentrations the pattern of hot and cold spots in figure 3(a), as well as the peaks and valleys in figure 3(b) tend to be at the same positions, it is plausible that these variations are artifacts caused by the imaging setup. In particular, they are likely originated by an inhomogeneity of the detector response in terms of energy deposition, which could not be completely corrected for through open field images and images of homogeneous PMMA plates. Considering this limitation, a substantial increase in WET values can be seen at a mass fraction of 4wt% compared to pure oil. The WET of the 10 mm PMMA was subtracted from the mean WET values in order to only consider the cavity. Contrast enhancement in terms of increased mean WET of 3.2%, 4.2% and 6.6% was hence found for the three mass fractions, respectively.

3.2. Contrast enhancement in pCT

3.2.1. pCT simulations of a cylindrical phantom

The central slice of the reconstructed pCT image for an imaging dose of 200 mGy of the water phantom with cylinders of varying gadolinium oxide concentrations with no background concentration is presented in figure 4(a). The solid red circles indicate the interfaces and the dashed circles represent the ROIs used for the determination of the CNR. Corresponding profiles through five of the cavities are shown in figure 4(b). Boundaries of the cavities and the ROIs are shown by the vertical solid and dashed lines, respectively. For all three reconstructed slices, an overview of the RSP voxel values within the cavities and the smaller ROIs for the pCT simulations without background concentration is given as a box plot in figure 4(c). Evidently, due to the spatial resolution of 0.5 mm predominantely dictated by multiple Coulomb scattering, the spread of the RSP values is much more pronounced when considering the entire region rather than only the reduced ROIs. While for the entire region the spread increases with larger gadolinium oxide concentration, it remains rather constant for the smaller ROIs.

According to a linear fit to the CNRs corresponding to the reduced ROIs, the minimum required concentrations to obtain a CNR $= 5$ are (2.7 ± 0.4)wt% and (2.4 ± 0.2)wt% for 100 and 200 mGy, respectively. With a background concentration of 0.2wt%, these values increase to (3.3 ± 0.4)wt% and (2.7 ± 0.3)wt% for the two imaging doses. When considering the entire cavities to account for their full detectability, the minimum concentrations increase to (3.7 ± 0.2)wt% and (2.9 ± 0.2)wt% (no background) and to (4.7 ± 0.8)wt% and (3.8 ± 0.3)wt% (with background) for the two imaging doses, respectively.

3.2.2. Murine pCT simulation

For the pre-clinical pCT simulation, axial slices through the center of the fictitious tumor volume for all studied gadolinium oxide concentrations and imaging dose values are presented in figure 5. Visually, an increased detectability, i.e. larger RSP values, is clearly obtained with both higher concentration and dose. The CNR determined for the entire tumor volume, as well as for the smaller ROI including a 1 mm margin, is shown in figures 6(a) and (b) for different concentrations and image doses. Similar to the previous analyses, a linear fit to the data points indicates the minimum concentration and dose required to fullfill the Rose criterion. For 80, 160 and 320 mGy, detectability of the smaller ROI is ensured at concentrations of 5.5, 3.3 and 2.3wt%, respectively. From the linear fit in figure 6(b) the imaging dose required for detectability for a given gadolinium oxide concentration can be estimated. If the concentration in the fictitious tumor volume is limited to e.g. 2wt%, 389 mGy would be required to detect the smaller ROI, and almost twice the dose (760 mGy) would be necessary to achieve full detectability of the entire tumor volume. For a mass fraction of 4wt%, the respective imaging doses would be 125 mGy and 248 mGy. Note that unlike in the simulated pCT

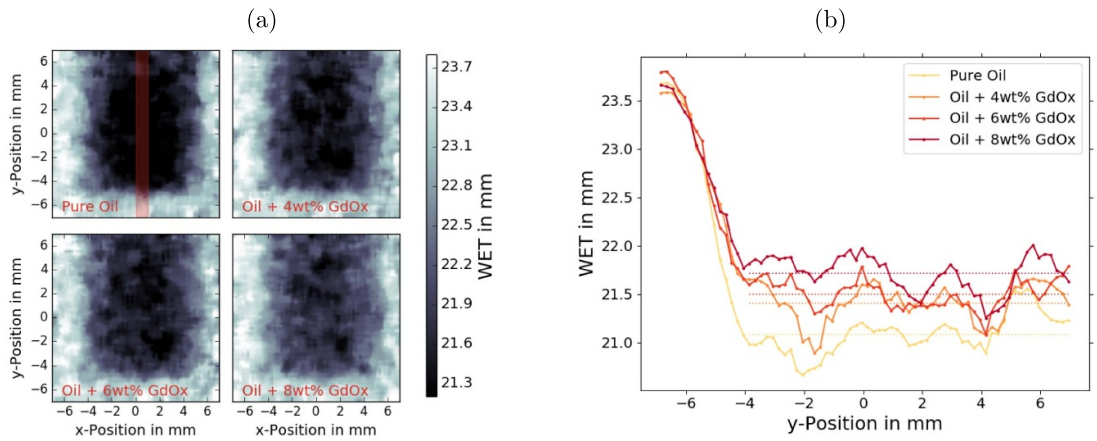

Figure 3. (a) Proton radiographies obtained at the Trento PTC using the MiniPIX-based imaging setup. WET profiles following the central cylinder axis (indicated by red bar) and averaged along 5 pixels are shown in (b). The dotted lines correspond to the mean WET of the profiles within the cavity. The *y*-axis is aligned from bottom to top.

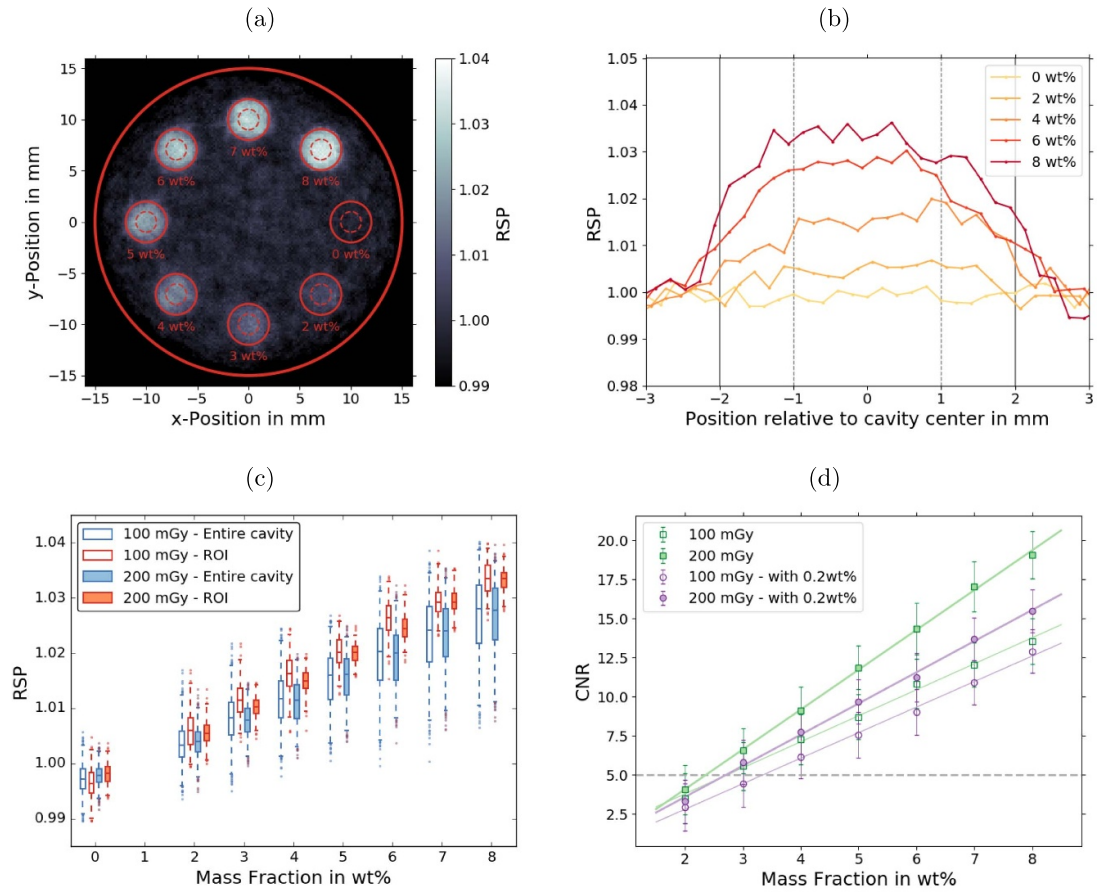

Figure 4. (a) Simulated pCT image of gadolinium oxide loaded water phantom (no background concentration). Phantom and cavity interfaces are highlighted by the solid red circles, dashed circles indicate the smaller ROIs with margin subtracted. Horizontal line profiles through 5 exemplary cavities within one reconstructed slice are shown in (b). The solid and dashed grey lines indicate the extension of the cavity and the cavity minus margin, respectively. In (c), the RSP values in the cavities are represented in a box plot. Whiskers are ranging from the 1st to 99th percentile. The CNR of the cavity minus margin is shown as a function of mass fraction in (d).

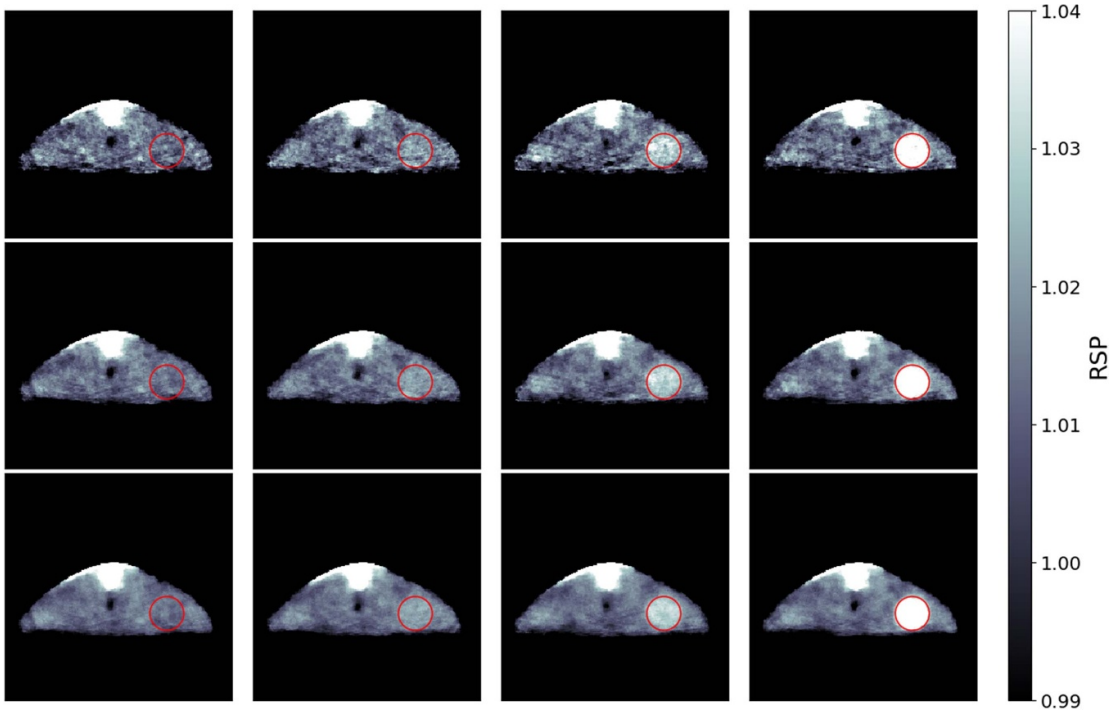

Figure 5. Axial slice of simulated murine pCT. The fictitious tumor volume is indicated by the red circles. Gadolinium oxide mass fractions of 0wt% (i.e. no contrast enhancement), 2wt%, 4wt% and 8wt% are respectively shown in the four columns. The three rows correspond to an imaging dose of 80, 160 and 320 mGy.

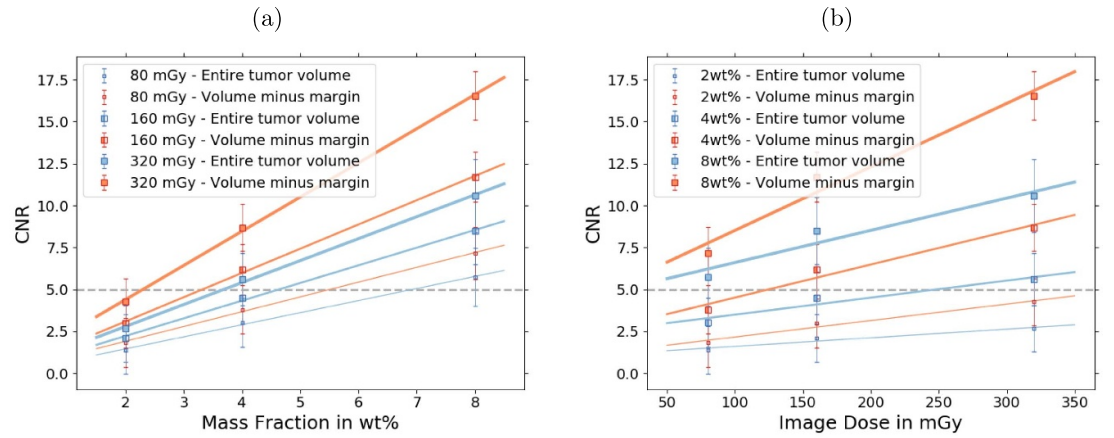

Figure 6. The CNR of the fictitious murine tumor volumes is plotted as a function of mass fraction (a) and dose (b). Solid lines correspond to linear fits to the data points.

of the cylindrical phantom, there was no background concentration of the contrast agent in the surrounding tissue.

3.3. Contrast enhancement in x-ray CBCT imaging

Detectability of the gadolinium oxide loaded features in xCT is already achieved at a considerably lower mass fraction as compared to the findings for pCT. As it can be seen in figures 7(a) and (b), the cavity filled with 0.5wt% can clearly be distinguished from the cavity filled with pure oil. In figure 7(c), HU values of the 50 central slices, corresponding to 13 mm, are summarized for the entire cavity and the smaller region of interest. The larger spread of HU values for higher mass fraction is due to the large HU gradient at the interface between cavity and PMMA phantom, as shown in figure 7(b). According to the linear fit to the extracted CNR values (figure 7(d)), the Rose criterion is already fullfilled at a mass fraction of 0.56wt% for the entire cavity. Considering a smaller ROI with subtracted margin, about one order of magnitude lower mass fraction seems to be sufficient for detectability.

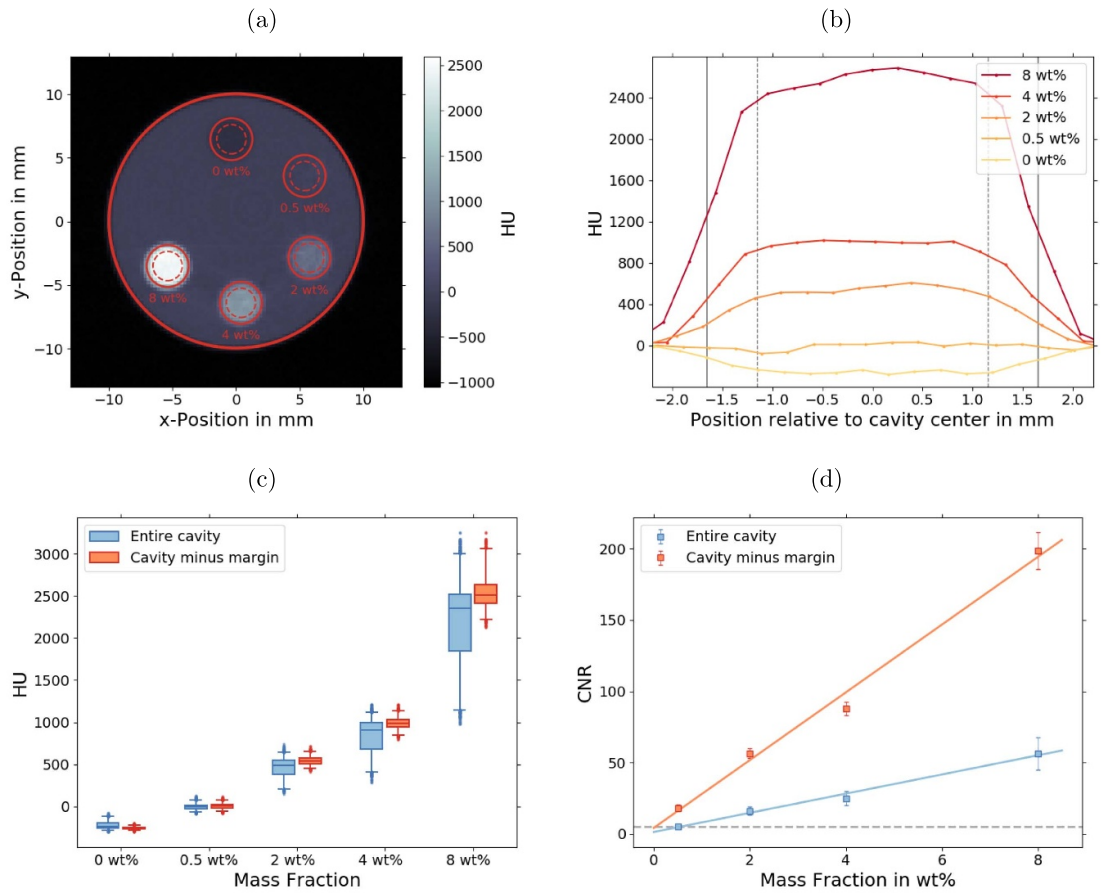

Figure 7. (a) Experimental x-ray CBCT image of gadolinium oxide loaded PMMA phantom. Phantom and cavity interfaces are highlighted by the solid red circles, dashed circles indicate the smaller ROIs with margin subtracted. Horizontal line profiles through the 5 cavities within one reconstructed slice are shown in (b). The solid and dashed grey lines indicate the extension of the cavity and the smaller ROI, respectively. In (c), the CT numbers of 50 central slices of the cavities are represented in a box plot. Whiskers are ranging from the 1st to 99th percentile. The CNR is shown as a function of mass fraction in (d).

4. Discussion

Within the past years, the interest in gadolinium-based nanoparticles both as radiosensitizers for radiation therapy and as contrast enhancement agents for diagnostic imaging has been continuously increasing. Particularly the possible multimodal use of gadolinium to enhance contrast in magnetic resonance imaging and x-ray imaging, including x-ray fluorescence imaging, offers a wide range of applications. The scope of our study was to further investigate, both experimentally and using MC simulations, the potential of gadolinium-based NPs as contrast agent in proton imaging (pRad and pCT). This imaging modality is not yet clinically available, but with increasing number of proton therapy facilities, prototype scanners for human patients (Bashkirov *et al* 2016, Esposito *et al* 2018) and small animals (Meyer *et al* 2020, Schneider *et al* 2022) are currently being developed at several research institutes worldwide. To provide a context for the results obtained in this study for proton imaging, comparative measurements were performed with an x-ray CBCT scanner of a commercial small animal x-ray irradiation platform.

Considerable contrast enhancement in terms of increased WET was found in our proton radiography experiments for the lowest investigated gadolinium oxide concentration of 4wt% and an estimated median imaging dose of 2 mGy. However, the determined WET increase of about 3.2% was considerably larger than the expected RSP increase based on MC simulations of plain slabs of dispersions (1.7% for 4wt%). A possible unbalance of scattering in PMMA versus gadolinium oxide dispersion might contribute to the difference. Yet, the most plausible explanation for this discrepancy might be the unequal gadolinium oxide mass fraction in the imaged vessel due to settling of the agglomerated nanoparticles. Settling of the nanoparticles is considerably slower in oil than in water and visually no inhomogeneity in the nanoparticle distribution could be observed during the experimental campaign. Nevertheless, a larger gadolinium oxide concentration in the imaged lower part of the vessel as compared to the upper part of it has to be expected. This is due to the delay between filling and start of data acquisition ($\approx$2 min) and the comparably long acquisition time of up to

15 min. Due to the limited detector size, only the lower part of the vessel was imaged (see figure 1(a)). By using a different proton imaging setup with shorter acquisition time and larger sensitive detector area covering the entire vessel, it might be possible to temporally and spatially resolve the gadolinium oxide concentration in the dispersion. Regardless of the possible bias due to settling, as well as the hot and cold spots in the two-dimensional WET distribution, the experimentally obtained radiographic data can confirm the feasibility of gadolinium oxide nanoparticles as contrast enhancement agent in proton imaging and complement the pCT simulation study.

The detectability of a contrast agent loaded structure in pCT for a given imaging setting depends on the one hand on the nanoparticle concentration and the imaging dose, and on the other hand on the choice of the ROI. If the goal of the nanoparticle administration is to localize an already known tumor volume in a tomographic scan, a gadolinium oxide concentration of 2wt% might already be sufficient, as shown in two independent in-silico studies with slightly different imaging settings tailored to the respective objectives. However, in order to delineate the entire tumor for e.g. quantitative information on the tumor growth, concentrations of 4wt% would be necessary at acceptable imaging doses of only a few hundred mGy. In a realistic scenario, the unavoidable background concentration of gadolinium oxide in the surrounding tissue will result in slightly increased values for either minimum concentration or required image dose. However, further possibilities of dose reduction preserving contrast agent detectability could be explored, featuring improvements of pCT instrumentation, data acquisition (e.g. through the so-called fluence modulation experimentally demonstrated by Dedes *et al* (2018) at clinical proton beam energies) and processing (e.g. making usage of prior information and artificial intelligence).

In CBCT imaging, the minimum required gadolinium oxide concentration is considerably lower than in proton imaging. The reason for the large difference can easily explained by the different underlying physics for both imaging modalities. In x-ray imaging the increased mass attenuation coefficient, caused by the higher cross-section of the photoelectric effect $\sigma_{p.e.}$ for high-Z materials is the basis of contrast enhancement. Due to the high atomic number of gadolinium ($Z = 64$) and the strong Z-dependence of $\sigma_{p.e.}$, already comparably low gadolinium concentrations in tissue result in a pronounced increase of the attenuation coefficient, especially in the x-ray energy range typically used for small animal imaging, which is slightly above the K-edge of gadolinium (50.2 keV). On the other hand, contrast enhancement in energy loss pCT is related to an increased RSP in the feature of interest, which in turn approximately depends linearly on its electron density. Since the Z/A ratio slightly decreases for a dispersion of gadolinium oxide and tissue compared to tissue without nanoparticles, the increased RSP is mainly a consequence of the higher tissue density caused by the uptake of gadolinium oxide in the targeted volume. According to FLUKA simulations, a mass fraction of e.g. 1wt% in water results in an RSP enhancement below 0.5% for a proton energy of 75 MeV. Improved contrast enhancement in proton imaging might be obtained when additionally considering scattering pCT, which potentially provides higher contrast images than conventional energy loss pCT (Plautz *et al* 2014). Due to edge enhancement, this strategy could prove beneficial especially for the delineation of gadolinium oxide loaded tumor volumes. The scattering length X_S as defined in Gottschalk (2010) inversely depends on $\rho Z^2/A$. Using the Bragg additivity rule for compounds or mixtures leads to reduction of X_S by about 6% when comparing 1wt% gadolinium oxide in water to pure water. However, at equal dose, reconstructed scattering pCT images show considerably higher noise than energy-loss pCT images (Krah *et al* 2020). Whether including this scattering information for contrast enhanced proton imaging can be beneficial hence needs to be investigated in a dedicated study.

Beyond the physical perspective of contrast enhancement in proton imaging using gadolinium-based nanoparticles, the question remains whether such gadolinium accumulation in the tumor volume can be achieved from a biological point of view. Although the answer to this question is beyond the scope of this study, a back-of-the-envelope calculation based on published literature may give an estimate on the biological feasibility. Considering a large tumor volume as used in our murine simulated pCT and assuming a tumor density close to the density of water, the tumor mass is in the order of 0.1 g. Hence, based on the minimum required concentration for the detection of the ROI at an imaging dose of 320 mGy, the mass of gadolinium oxide tumor uptake needs to exceed 2.3 mg. In Sancey *et al* (2015), non-tumor-bearing mice received an intraveneously injected therapeutic dose (TD) of the gadolinium-based nanoparticles AGuIX® of 8 μmol gadolinium ions in a single administration. With a total injected gadolinium mass of 1.26 mg, this would correspond to only about half the required amount of gadolinium. The maximum tolerated dose (MTD) of these nanoparticles in mice was determined to be about 10-fold higher than the TD (Sancey *et al* 2015), hence about 5 times more than required for detection of the ROI. However, with passive targeting the tumor uptake is below 1% of the injected dose in animal models (Lux *et al* 2019). Therefore, considering the MTD and an imaging dose of 320 mGy, the obtained concentration in the tumor volume would still be a factor of 20 lower than required as contrast enhancement in pCT, whereas detectability in xCT could already be feasible. It has to be stressed that the fictitious tumor volume in the presented pCT simulation was chosen

rather large and up to one order of magnitude smaller volumes would still be relevant in pre-clinical murine studies (Stegen *et al* 2020). Increased tumor uptake could either be achieved by actively targeting nanoparticles (e.g. Morlieras *et al* 2013), or by alternative administration routes like intratumoral injection for easily accessible tumors (Miladi *et al* 2015) or intraperitoneal administration, which presumably leads to a slower renal excretion (Hu *et al* 2017). In fact, this could be of interest to also explore the effect of high-Z nanoparticles on radiosensitization.

Finally, the potential of scattering pCT or particle-induced x-ray emission (PIXE) for improved tumor localization might be a promising route to be explored in dedicated studies. Hence, future work is needed to further explore the potential of nanoparticles in the context of small animal proton imaging and to identify the acceptable concentrations yielding levels of enhancement which would justify the additional workload and possible impact on the animal.

5. Conclusion

In the present study, gadolinium based nanoparticles were investigated as a multimodal contrast enhancement agent for proton imaging in the context of small animal irradiation. To this aim, the detectability of small gadolinium oxide loaded structures in pCT was examined as a function of imaging dose and concentration using a realistic MC implementation of a small animal pCT system. With no or low background concentration in the surrounding tissue, full detectability of the entire structure requires a gadolinium oxide mass fraction of approximately 4wt% at an imaging dose of a few hundred mGy. Lower mass fractions and/or imaging doses may be sufficient if the aim is to localize the structure, without extracting quantitative information on its volume. For a comparable imaging dose, localization of gadolinium oxide loaded structures in small animal x-ray imaging requires a considerably lower nanoparticle concentration (<0.1wt%). Achieving nanoparticle concentrations above 1wt% *in-vivo* seems challenging, however active targeting or intratumoral injection could potentially lead to a sufficient concentration for significant contrast enhancement in proton imaging. Finally, the potential of scattering pCT or PIXE for improved tumor localization might be a promising route to be explored in further studies.

Data availability statement

The data cannot be made publicly available upon publication because they are not available in a format that is sufficiently accessible or reusable by other researchers. The data that support the findings of this study are available upon reasonable request from the authors.

Acknowledgments

This work was funded by the European Research Council (SIRMIO, Grant No. 725539). We want to thank Chiara Gianoli, Georgios Dedes, Frank Verhaegen, Nick Staut and Merle Reinhart for fruitful discussions.

ORCID iDs

Matthias Würl https://orcid.org/0000-0003-3044-449X
Guyue Hu https://orcid.org/0009-0004-0821-7236
Sebastian Meyer https://orcid.org/0000-0002-2510-7045
Jonathan Bortfeldt https://orcid.org/0000-0002-0777-985X
Guillaume Landry https://orcid.org/0000-0003-1707-4068
Carlos Granja https://orcid.org/0000-0002-4398-1553
Cristina Oancea https://orcid.org/0000-0002-1745-9702
Francesco Tommassino https://orcid.org/0000-0002-8684-9261
Katia Parodi https://orcid.org/0000-0001-7779-6690

References

Ahmad W, Xu W, Kim S, Baeck J, Chang Y, Bae J E, Chae K S, Park J, Kim T and Lee G 2015 Potential dual imaging nanoparticle: Gd_2O_3 nanoparticle *Sci. Rep.* **5** 8549

Bashkirov V A, Johnson R P, Sadrozinski H F W and Schulte R W 2016 Development of proton computed tomography detectors for applications in hadron therapy *Nucl. Instrum. Methods Phys. Res.* A **809** 120–9

Böhlen T, Cerutti F, Chin M, Fassó A, Ferrari A, Ortega P, Mairani A, Sala P, Smirnov G and Vlachoudis V 2014 The FLUKA code: developments and challenges for high energy and medical applications *Nucl. Data Sheets* **120** 211–4

Bridot J L *et al* 2007 Hybrid gadolinium oxide nanoparticles: multimodal contrast agents for *in vivo* imaging *J. Am. Chem. Soc.* **129** 5076–84

Burgess A E 1999 The rose model, revisited *J. Opt. Soc. Am.* A **16** 633–46
Cho S H, Jones B L and Krishnan S 2009 The dosimetric feasibility of gold nanoparticle-aided radiation therapy (GNRT) via brachytherapy using low-energy gamma-/x-ray sources *Phys. Med. Biol.* **54** 4889–905
Cole L E, Ross R D, Tilley J M, Vargo-Gogola T and Roeder R K 2015 Gold nanoparticles as contrast agents in x-ray imaging and computed tomography *Nanomedicine* **10** 321–41
Cormack A M and Koehler A M 1976 Quantitative proton tomography: preliminary experiments *Phys. Med. Biol.* **21** 560–9
Dedes G, Johnson R P, Pankuch M, Detrich N, Pols W M A, Rit S, Schulte R W, Parodi K and Landry G 2018 Experimental fluence-modulated proton computed tomography by pencil beam scanning *Med. Phys.* **45** 3287–96
Dunning C and Bazalova-Carter M 2020 Design of a combined x-ray fluorescence computed tomography (CT) and photon-counting CT table-top imaging system *J. Instrum.* **15** 06031–06031
Esposito M *et al* 2018 PRaVDA: the first solid-state system for proton computed tomography *Phys. Medica* **55** 149–54
Feldkamp L A, Davis L C and Kress J W 1984 Practical cone-beam algorithm *J. Opt. Soc. Am.* A **1** 612–9
Ferrari A, Sala P R, Fassó A and Ranft J 2005 FLUKA: a multi-particle transport code *CERN Yellow Reports: Monographs* CERN-2005-10, INFN/TC_05/11, SLAC-R-773 (OSTI Information Bridge Server, CERN Document Server)
Gottschalk B 2010 On the scattering power of radiotherapy protons *Med. Phys.* **37** 352–67
Granja C, Kudela K, Jakubek J, Krist P, Chvatil D, Stursa J and Polansky S 2018 Directional detection of charged particles and cosmic rays with the miniaturized radiation camera minipix timepix *Nucl. Instrum. Methods Phys. Res.* A **911** 142–52
Hainfeld J F, Slatkin D N, Focella T M and Smilowitz H M 2006 Gold nanoparticles: a new x-ray contrast agent *Br. J. Radiol.* **79** 248–53
Hainfeld J F, Slatkin D N and Smilowitz H M 2004 The use of gold nanoparticles to enhance radiotherapy in mice *Phys. Med. Biol.* **49** N309–15
Hu G 2021 Expansion and validation of an image reconstruction framework for a novel small-animal proton CT system *PhD Thesis* TU Munich
Hu P, Cheng D, Huang T, Banizs A, Xiao J, Liu G, Chen Q, Wang Y, He J and Shi H 2017 Evaluation of novel ^{64}Cu-labeled theranostic gadolinium-based nanoprobes in HepG2 tumor-bearing nude mice *Nanoscale Res. Lett.* **12** 523
Jakubek J 2011 Precise energy calibration of pixel detector working in time-over-threshold mode *Nucl. Instrum. Methods Phys. Res.* A **633** S262–6
Johnstone C D and Bazalova-Carter M 2018 MicroCT imaging dose to mouse organs using a validated Monte Carlo model of the small animal radiation research platform (SARRP) *Phys. Med. Biol.* **63** 115012
Kim M M, Irmen P, Shoniyozov K, Verginadis I I, Cengel K A, Koumenis C, Metz J M, Dong L and Diffenderfer E S 2019 Design and commissioning of an image-guided small animal radiation platform and quality assurance protocol for integrated proton and x-ray radiobiology research *Phys. Med. Biol.* **64** 135013
Kozłowska W S, Böhlen T T, Cuccagna C, Ferrari A, Fracchiolla F, Magro G, Mairani A, Schwarz M, Vlachoudis V and Georg D 2019 Fluka particle therapy tool for Monte Carlo independent calculation of scanned proton and carbon ion beam therapy *Phys. Med. Biol.* **64** 075012
Krah N, Quiñones C T, Létang J M and Rit S 2020 Scattering proton CT *Phys. Med. Biol.* **65** 225015
Lin Y, McMahon S J, Scarpelli M, Paganetti H and Schuemann J 2014 Comparing gold nano-particle enhanced radiotherapy with protons, megavoltage photons and kilovoltage photons: a Monte Carlo simulation *Phys. Med. Biol.* **59** 7675–89
Llopart X, Ballabriga R, Campbell M, Tlustos L and Wong W 2007 Timepix, a 65k programmable pixel readout chip for arrival time, energy and/or photon counting measurements *Nucl. Instrum. Methods Phys. Res.* A **581** 485–94
Lux F *et al* 2019 AGuIX® from bench to bedside—transfer of an ultrasmall theranostic gadolinium-based nanoparticle to clinical medicine *Br. J. Radiol.* **92** 20180365
Meyer S 2019 On the clinical potential of ion computed tomography with different detector systems and ion species *PhD Thesis* LMU Munich
Meyer S, Bortfeldt J, Lämmer P, Englbrecht F, Pinto M, Schnürle K, Würl M and Parodi K 2020 Optimization and performance study of a proton CT system for pre-clinical small animal imaging *Phys. Med. Biol.* **65** 155008
Miladi I *et al* 2015 Combining ultrasmall gadolinium-based nanoparticles with photon irradiation overcomes radioresistance of head and neck squamous cell carcinoma *Nanomed. Nanotechnol. Biol. Med.* **11** 247–57
Morlieras J *et al* 2013 Functionalization of small rigid platforms with cyclic RGD peptides for targeting tumors overexpressing $\alpha_v\beta_3$-integrins *Bioconjug. Chem.* **24** 1584–97
Olsansky V, Granja C, Oancea C, Mackova A, Havranek V, Chvatil D and Bila J 2022 Spectral-sensitive proton radiography of thin samples with the pixel detector Timepix3 *J. Instrum.* **17** C04016
Parodi K *et al* 2019 Towards a novel small animal proton irradiation platform: the SIRMIO project *Acta Oncol.* **58** 1470–5
Parodi K, Ferrari A, Sommerer F and Paganetti H 2007 Clinical CT-based calculations of dose and positron emitter distributions in proton therapy using the FLUKA Monte Carlo code *Phys. Med. Biol.* **52** 3369–87
Plautz T *et al* 2014 200 MeV proton radiography studies with a hand phantom using a prototype proton CT scanner *IEEE Trans. Med. Imaging* **33** 875–81
Rajaee A, Wang S, Zhao L, Wang D, Liu Y, Wang J and Ying K 2019 Multifunction bismuth gadolinium oxide nanoparticles as radiosensitizer in radiation therapy and imaging *Phys. Med. Biol.* **64** 195007
Rose A 1973 *Vision: Human and Electronic* (Springer)
Sancey L *et al* 2015 Long-term *in vivo* clearance of gadolinium-based AGuIX nanoparticles and their biocompatibility after systemic injection *ACS Nano* **9** 2477–88
Schneider M *et al* 2022 Combined proton radiography and irradiation for high-precision preclinical studies in small animals *Front. Oncol.* **12** 982417
Schuemann J *et al* 2020 Roadmap for metal nanoparticles in radiation therapy: current status, translational challenges and future directions *Phys. Med. Biol.* **65** 21RM02
Schulte R W, Bashkirov V, Loss Klock M C, Li T, Wroe A J, Evseev I, Williams D C and Satogata T 2005 Density resolution of proton computed tomography *Med. Phys.* **32** 1035–46
Schulte R, Bashkirov V, Li T, Liang Z, Sadrozinski H W and Williams D 2004 Nanoparticle-enhanced proton computed tomography: a Monte Carlo simulation study *2004 2nd IEEE Int. Symp. on Biomedical Imaging: Nano to Macro (IEEE Cat No. 04EX821)* vol 2 pp 1354–6
Sidebottom R B *et al* 2021 Contrast-enhanced proton radiographic sensitivity limits for tumor detection *J. Med. Imaging* **8** 1–16
Stegen B *et al* 2020 Contrast-enhanced, conebeam CT-based, fractionated radiotherapy and follow-up monitoring of orthotopic mouse glioblastoma: a proof-of-concept study *Radiat. Oncol.* **15** 19

Tillner F et al 2016 Precise image-guided irradiation of small animals: a flexible non-profit platform *Phys. Med. Biol.* **61** 3084–108
Tommasino F et al 2017 Proton beam characterization in the experimental room of the Trento Proton Therapy facility *Nucl. Instrum. Methods Phys. Res.* A **869** 15–20
Verhaegen F et al 2018 ESTRO ACROP: technology for precision small animal radiotherapy research: optimal use and challenges *Radiother. Oncol.* **126** 471–8
Verhaegen F, Granton P and Tryggestad E 2011 Small animal radiotherapy research platforms *Phys. Med. Biol.* **56** R55–R83
Verry C et al 2019 Treatment of multiple brain metastases using gadolinium nanoparticles and radiotherapy: NANO-RAD, a phase I study protocol *BMJ Open* **9** e023591
Vlachoudis V 2009 FLAIR: a powerful but user friendly graphical interface for FLUKA *Proc. Int. Conf. on Mathematics, Computational Methods & Reactor Physics (M&C 2009)* (*Saratoga Springs, New York, 2009*)
Wong J et al 2008 High-resolution, small animal radiation research platform with x-ray tomographic guidance capabilities *Int. J. Radiat. Oncol. Biol. Phys.* **71** 1591–9
Würl M, Englbrecht F, Parodi K and Hillbrand M 2016 Dosimetric impact of the low-dose envelope of scanned proton beams at a ProBeam facility: comparison of measurements with TPS and MC calculations *Phys. Med. Biol.* **61** 958–73
Würl M, Schnürle K, Bortfeldt J, Oancea C, Granja C, Verroi E, Tommasino F and Parodi K 2020 Proton radiography for a small-animal irradiation platform based on a miniaturized timepix detector *2020 IEEE Nuclear Science Symp. and Medical Imaging Conf. (NSS/MIC)* pp 1–6
Yang Y, Armour M, Wang K K-H, Gandhi N, Iordachita I, Siewerdsen J and Wong J 2015 Evaluation of a cone beam computed tomography geometry for image guided small animal irradiation *Phys. Med. Biol.* **60** 5163